Ligand-Directed Valence Band Engineering in Pb^{2+} Hybrid Crystals: Achieving Dispersive Bands and Shallow Valence Band Maximum

Daiki Umeyama* and Soshi Iimura

National Institute for Materials Science, 1-1 Namiki, Tsukuba 305-0044, Japan.

ABSTRACT: While crystalline hybrid solids hold great potential as novel semiconductors, most semiconductive hybrids utilize transition metal ions, which inherently limit carrier mobility due to the small band dispersion derived from the d orbitals. The filled s orbitals of post-transition metal ions offer the potential to design dispersed valence bands, but a method to translate the local structure design of these metal ions to valence band engineering is still in development. This study focuses on Pb^{2+}-containing hybrid crystals, developing a simple strategy to control Pb^{2+} coordination geometry through the molecular design of azole ligands. By pre-programming the coordination number of Pb^{2+} with azolate ligands, we succeeded in obtaining an isotropic coordination environment at a higher coordination number, resulting in a dispersed valence band and shallow valence band maximum while having a wide band gap. Detailed analysis of the band structures reveals that the energy levels and symmetry of the molecular orbitals of the anions play an important role in realizing these antinomic properties. This ligand-directed approach achieves both isotropy and covalency in the coordination bond by exploiting the diversity of molecular orbitals. Our findings provide a foundation for future design strategies to optimize electronic structures in hybrid materials, advancing their application in semiconductive devices.

1. INTRODUCTION

The ability to control the electronic structure of solids is central to materials science because it is the primary determinant of charge transport properties. The control of carrier concentration and mobility is the essential factor that enables the application of semiconductors in devices.[1] In particular, for sensing and photocatalysis, organic-inorganic hybrid semiconductors have great potential due to their tailorable surface area and catalytic sites based on metal selection and ligand design.[2–6] The fundamental methods and knowledge for semiconducting hybrid solids have been accumulated for this realization.[7] In the field of coordination polymers (CPs) and metal-organic frameworks (MOFs), reports of semiconductive CPs and MOFs have increased over the years. The majority of these materials consist of transition metal (TM) ions, and electronic communication between inorganic and organic motifs is achieved by d-p or d-π orbital interaction.[8–10] Proper design of the ligands and their combination with the right metal ions makes it possible to create carriers and control their concentration by doping.[11,12]

While the systematic study of TM-based CPs and MOFs advances science of semiconductive hybrid materials, the use of TM ions severely limits the ability to control the carrier mobility. This is because the contract nature of the d orbitals of TM ions intrinsically leads to small band dispersion.[13] Thus, the semiconducting properties of these hybrid materials have depended primarily on the control of the carrier concentration, leaving the control of the mobility behind. The tendency is more pronounced in valence bands, since conduction bands can be derived from the empty s orbitals of TM ions.[14] In this context, CPs and MOFs with post-transition metal (pTM) ions with ns^2np^0 electronic configurations (e.g., Pb^{2+}, Sn^{2+}, *etc*.) are of particular interest, which allow us to build dispersive valence bands using the antibonding interaction between filled metal orbitals and filled anion orbitals.[15,16] Isotropic and spatially extended *n*s orbitals of these metals are expected to give more dispersive bands than TM-based materials, resulting in smaller effective mass of holes.

Although not as common as structures with TM ions, many CPs and MOFs with pTM ions have also been reported.[17] However, despite the assumed isotropy of the s orbitals, the coordination geometry of the pTM ions is often distorted, which is a result of "stereochemically active lone pairs (LPs)".[18,19] The origin of LP formation is known to be the mixing of the metal *n*p states to the *n*s state,[20,21] and it is important to control the s-p hybridization of pTM ions to achieve desired properties. While factors such as the coordination number of pTM ions and steric hindrance of ligands are known to influence the LP activity in CPs and MOFs,[22–24] no clear concept has been established to translate these findings into the engineering of the valence bands of these hybrids. This is due to the lack of a precise strategy for programming the coordination number and a deep understanding of the interactions between pTM ions and ligands. As a result, the coordination geometry of pTM ions in these hybrids is in some aspects determined by chance, making it difficult to relate the ligand design to the electronic band structures of the pTM hybrids, regardless of the preservation of the isotropy of the metal s orbital.[25–28] Addressing these issues is an important challenge for the design of valence bands using occupied metal s orbitals in hybrid materials.

In this article, we focus on Pb^{2+} containing hybrid crystals and show a simple but effective strategy to actively control the coordination geometry of Pb^{2+}, which enables the valence band engineering. Importantly, we will show that the orbital mixing in hybrid solids does not need to be considered beforehand to preserve the isotropy of the Pb-6s orbital; we only need to control the coordination number of Pb^{2+}. We demonstrate that we can pre-program the coordination number of Pb^{2+} by the molecular design of anionic ligands. This method causes the Pb^{2+} to adopt a high coordination number by ligand design, thereby preserving the isotropic character of the filled 6s orbital. We show that this results in a more dispersed valence band and a smaller effective mass of holes, accompanied by a shallow valence band maximum. We will clarify how these molecules interact with the Pb^{2+} and dominate the band dispersion on the basis of detailed analysis of the wave functions of these hybrids. Unlike the TM-based systems, where d-p interactions are dominant, importance of σ-type interactions will be highlighted. We will also show the unique advantages of hybrid materials that result from the diversity of molecular orbitals (MOs).

2. CONCEPT AND METHOD

There is a useful classification of the coordination structure of the Pb^{2+}: "hemidirected" and "holodirected". In hemidirected structures, the bonds to ligand atoms are directed throughout only part of an encompassing globe, whereas in holodirected structures, the bonds to ligand atoms are distributed throughout the entire surface of the globe.[29] Hemidirected structures are associated with stereochemically active LPs, since the activity is obvious from the coordination geometry. A localized band structure can arise in an active LP (s-p hybridized) structure due to the mixing of the p orbitals, which induces directional orbital overlap and weakens the band dispersion compared to the omnidirectional s orbitals. The directionality of the p orbitals allows the LP electrons to avoid interacting with other orbitals, resulting in a nonbonding character or reduced antibonding interaction. Thus, being holodirected is a necessary (but not always sufficient) condition for suppressing LP activity and obtaining a dispersive valence band.

One of statistical studies of Cambridge Structural Database (CSD) suggests that the coordination geometry of the discrete complexes of Pb^{2+} is always hemidirected if the coordination number of Pb^{2+} (n_C) is 5 or less.[29] In contrast, Pb^{2+} complexes with $n_C \geq 6$ are about 70% holodirected, and with increasing n_C, more likely to have the holodirected geometry. This trend is also observed in extended Pb^{2+} structures (CPs and MOFs).[22,24] Another comprehensive study of CSD combined with density functional theory (DFT) revealed that the LP activity gradually decreases (accompanied by a decreasing Pb-6p contribution to the LP) with increasing n_C.[30] These findings imply that we can control the LP activity of the Pb^{2+} (and thus the degree of valence band dispersion) in a network structure by changing the n_C. However, just increasing the number of the donor site of ligands does not necessarily give us the control over n_C for dispersed bands. This is partially because some donor atoms such as the oxygen (O) of carboxylate provide an opportunistic n_C. This causes the n_C defined by such a ligand differ case-by-case even in a single structure.[22,24,25]

We hypothesized that the n_C in Pb^{2+} containing binary hybrids could be predetermined by using molecular anions in which the number of coordination points is well defined. This assumes that all available coordination sites in the ligand molecule work as donors, which we will show to be true later. We focused on molecules containing nitrogen (N) as a donor site and decided to use azoles, which can change the number of N atoms in the five-membered ring while having an equal or similar basicity on each N atom[31] (Scheme 1A). Unlike oxygen-based ligands, there is only single pair of unshared electrons on the N atom of the azoles when written in the Lewis structures. Therefore, a single N site is not supposed to bridge metal ions. This indicate that each N site adds only one coordination number to a Pb^{2+} ion, representing the well-defined character of the ligand. We used three azoles (HAz) that allow us to vary the number of N atoms, namely 1*H*-tetrazole (HTt), 1,2,4-triazole (HTr), and, imidazole (HIm) to complex with Pb^{2+} ions. These aromatic amines can behave as monovalent anions (Az^-) by deprotonating the hydrogen on the N atom. Since the charge balance in these binary systems requires the composition formula to be $Pb(Az)_2$, the n_C is fixed to be twice the number of N atoms in the azoles. Thus, the n_C of three compounds is expected to be 8 (Az = Tt), 6 (Tr), and 4 (Im), respectively (Scheme 1B).

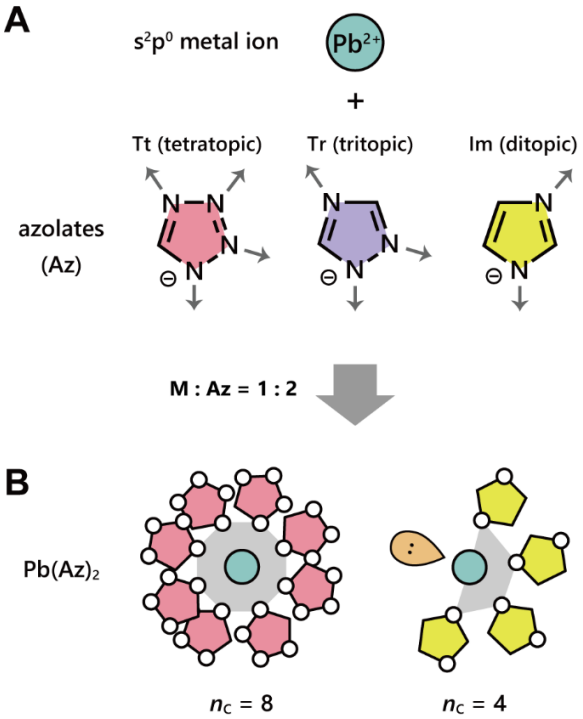

Scheme 1. Concept for defining the coordination number (n_C) of Pb^{2+}. (A) Three Az anions used in this study to form complex with Pb^{2+}. (B) Stoichiometry of $Pb(Az)_2$ requires n_C to be twice the number of N atoms in the Az anions.

3. RESULTS

Desired compounds were synthesized by mixing the preformed Az^- anions, deprotonated by potassium methoxide or hydroxide, with Pb^{2+} salts under solvothermal conditions, yielding colorless crystals (see details in Supporting Information). Structural analysis based on single-crystal X-ray diffraction (XRD) revealed that the prepared crystals were new binary compounds with the general formula $Pb(Az)_2$ (Figure 1A, B, C; Az = Tt, Tr, Im). Importantly, the n_C in these structures found to be 8 (Az = Tt), 6 (Tr), and 4 (Im), confirming the principle of ligand-directed control of the coordination number. Note that some of the N-donors of Az ligands may remain uncoordinated in binary azolate frameworks with TM ions due to their relatively rigid coordination number and geometry.[32,33] The fact that the ligands can define the n_C of $Pb(Az)_2$ reflects the flexibility of the coordination structure of Pb^{2+}, as described in the literature.[26,29,30]

We also succeeded in preparing powder crystals of $Pb(Az)_2$ by solvothermal synthesis, whose phase purity was confirmed by elemental analysis and powder XRD measurement (Figure S1 in SI). These are white powders whose optical absorption onsets are at 3.7 eV (Az = Tt), 4.1 eV (Tr), and 3.5 eV (Im), respectively, revealed by diffuse reflectance measurement of the powders (Figure S2 in SI).

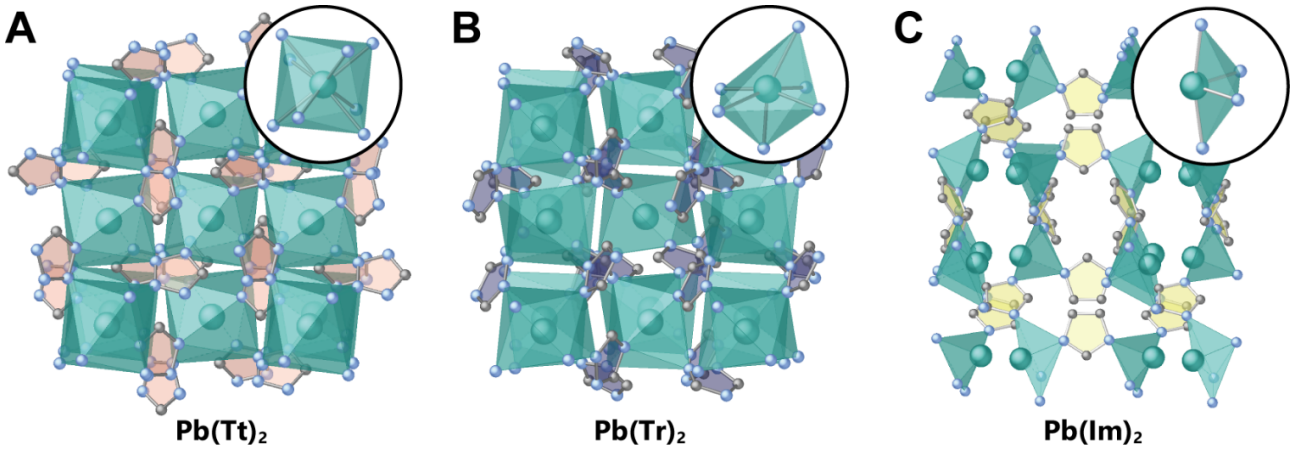

Figure 1. Crystal structures of (A) $Pb(Tt)_2$, (B) $Pb(Tr)_2$, and (C) $Pb(Im)_2$ determined by single-crystal X-ray diffraction. Green, Blue, and gray spheres represent Pb, N, C atoms, respectively. H atoms are omitted for clarity. Insets show local coordination geometry of Pb atoms.

3.1 Large n_C Results in Suppressed LP Activity and Dispersive Valence Bands in $Pb(Tt)_2$.

The coordination geometry of Pb^{2+} in $Pb(Tt)_2$ (n_C = 8) and $Pb(Tr)_2$ (n_C = 6) is best described as a triangulated dodecahedron and a distorted octahedron, respectively. The coordination geometry of Pb^{2+} is highly distorted in $Pb(Im)_2$ (n_C = 4) and all the coordinating N atoms are biased to one side of the coordination hemisphere. It is apparent that the Pb^{2+} ions have active LPs in $Pb(Tr)_2$ and $Pb(Im)_2$, while not in $Pb(Tt)_2$ (Figure 1, insets). Through analysis of electron density map and geometric coordinate, we will show that the LP activity is almost completely diminished in $Pb(Tt)_2$ while $Pb(Tr)_2$ and $Pb(Im)_2$ have significant LP (see Discussion). Thus, although the design principle of the molecular anion is very simple, forcing a coordination number is a powerful method to control the activity of the LPs of Pb^{2+}.

The suppressed LP in $Pb(Tt)_2$ suggests that s-p hybridization is minimal and therefore large valence band dispersion is expected in this compound. We used PBE hybrid functional with spin-orbit coupling (SOC) as implemented in the VASP code to calculated band structures of $Pb(Az)_2$ (Figure 2).[34–36] We notice that the dispersion of the valence band of $Pb(Tt)_2$ is significantly larger than those of $Pb(Tr)_2$ and $Pb(Im)_2$, which is consistent with the expected Pb-6s character in $Pb(Tt)_2$ near the valence band maximum (VBM). The degree of valence band dispersion is quantified by estimating the effective mass of holes(m_h*) of $Pb(Az)_2$. The calculated m_h* of $Pb(Tt)_2$ at the VBM is 1.3 (Z → P), 1.3 (Z → Γ), and 1.7 (Z → N). Note that $Pb(Tt)_2$ has a relatively small and isotropic m_h* for a hybrid compound. The m_h* of

$Pb(Tr)_2$ and $Pb(Im)_2$ are heavier and more anisotropic. For example, m_h* of $Pb(Im)_2$ at VBM is 2.3 (Γ → B) and 17 (Γ → Z).

3.2 Photo Excited Carriers Are Mobile in $Pb(Tt)_2$.

The small and isotropic m_h* of $Pb(Tt)_2$ is the quality required for a p-type semiconductor. As described later, the calculated energy position of the VBM of $Pb(Tt)_2$ relative to the vacuum level is in the range where p-doping can happen.[37] Nonetheless, how to p-dope the crystal is a nontrivial synthetic challenge and should be the subject of another future study. Here, we briefly show how the transport properties of $Pb(Tt)_2$ changes with carrier generation by photoexcitation.

The conductance of the crystal was measured by attaching two-point silver contacts to a single crystal of $Pb(Tt)_2$ at ambient temperature. We observed that the current was significantly increased by UVB irradiation (Figure 3). This photo response was confirmed to be reversible without pronounced hysteresis, as we observed that a dark measurement after an illuminated scan (and vice versa) was not affected by the previous scan (Figure S3A, 3C in SI). The *I-V* relationship under irradiated condition outside the range of ±1 V is non Ohmic and the current appears to saturate, which possibly occurs due to the energy transfer from accelerated carriers to lattice vibrations.[38] Under dark conditions, fitting of the linear region of the *I-V* curve gives a conductance (G) of $G^{dark} = 2.12(4)\times10^{-14}$ S (Figure S3B in SI). Under the irradiation of the UVB band (4.1–5.2 eV), the conductance increased about three orders of magnitude to $G^{UVB} = 1.65(3)\times10^{-11}$ S (Figure S3D in SI). We also observed that irradiation of a visible band (1.8–3.1 eV) had little effect on the conductivity (Figure S3E in SI). In addition, a $Pb(Tt)_2$ crystal with vapor-deposited gold contacts exhibited a similar photo response (Figure S4). These results indicate that the photo response originates from the bulk and that $Pb(Tt)_2$ exhibits semiconducting properties when carriers are generated by an above-gap photoexcitation.

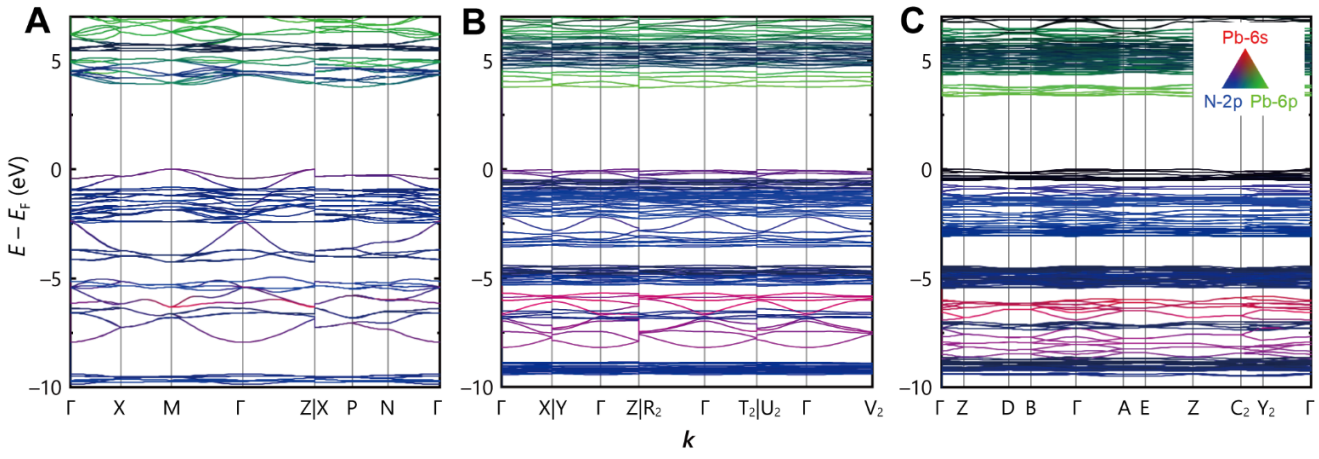

Figure 2. Electronic band structures of (A) $Pb(Tt)_2$, (B) $Pb(Tr)_2$, and (C) $Pb(Im)_2$ (E_F: Fermi energy). Orbital characters in the band structures are colored by red (Pb 6s), green (Pb 6p), and blue (N 2p).

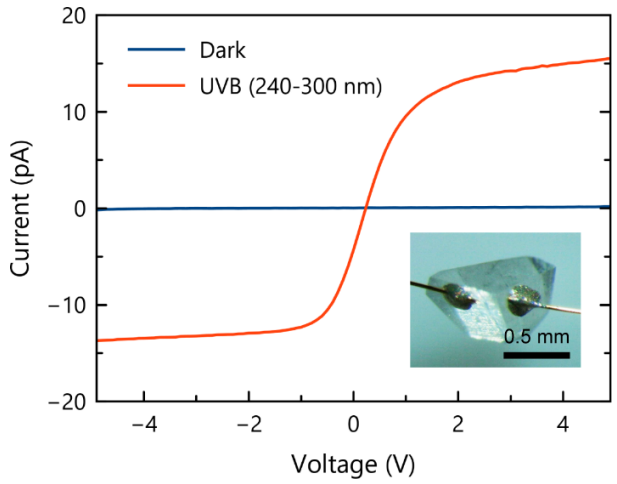

Figure 3. Room-temperature *I-V* curves of a $Pb(Tt)_2$ single crystal under dark (blue) and UVB irradiation (red).

4. DISCUSSION

4.1 Mechanism of the LP Suppression and Formation in $Pb(Az)_2$.

The crystal structures of $Pb(Az)_2$ suggest that the coordination geometry of $Pb(Tr)_2$ and $Pb(Im)_2$ are distorted by active LPs while $Pb(Tt)_2$ is not. The absence of the LP activity in $Pb(Tt)_2$ suggests that the 6s character of the valence electrons of Pb^{2+} is preserved. Conversely, the valence bands of $Pb(Im)_2$ and $Pb(Tr)_2$ near the band edges should contain a non-trivial amount of the 6p character. These characteristics are visualized by electron density maps and the partial density of states (PDOS) of $Pb(Az)_2$ (Figure 4). The electron densities were mapped using the result without SOC for the states between −12 and 0 eV and plotted in the plane spanned by the Pb–LP vector and the Pb–N vector of the shortest bond length in each crystal (see SI for the SOC exclusion). $Pb(Tt)_2$ shows symmetric electron density around the Pb^{2+} ions, while $Pb(Im)_2$ and $Pb(Tr)_2$ show asymmetric electron densities along the Pb–LP vectors as expected.

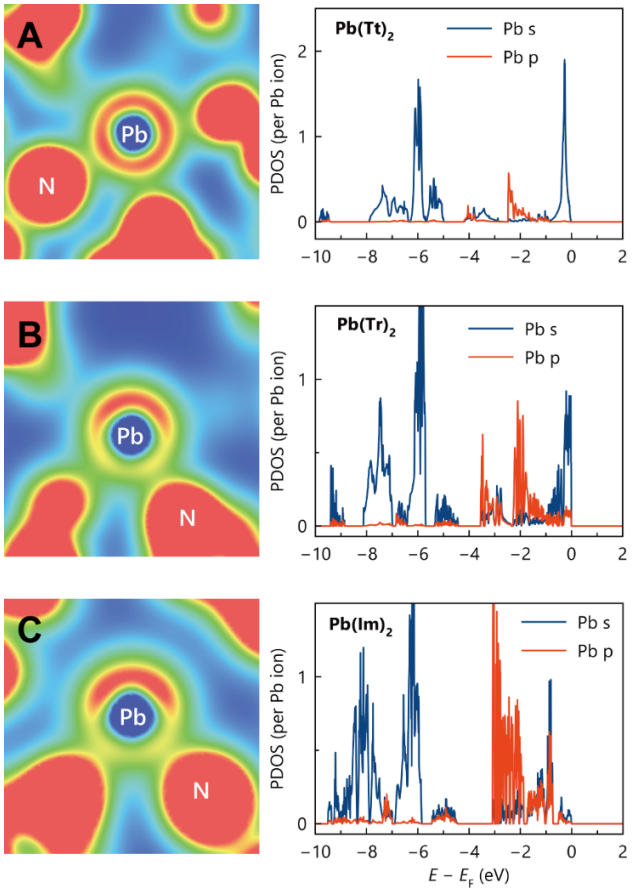

Figure 4. Partial electron densities from −12 to 0 eV and PDOS of Pb orbitals for (A) $Pb(Tt)_2$, (B) $Pb(Tr)_2$, and (C) $Pb(Im)_2$. The electron densities are plotted in the plane spanned by the LP vector and the shortest Pb–N vector. Contour levels are between 0 (blue) to 0.05 a_0^{-3} (red) (a_0: Bohr radius).

By analyzing the PDOS of $Pb(Az)_2$, we can conclude that the strong anisotropy is the result of the Pb-6p orbital contribution to the valence band. As seen in Figure 4, the PDOS of $Pb(Im)_2$ and $Pb(Tr)_2$ show significant amount of Pb-6p character from −4 to 0 eV, overlapped with the PDOS of Pb 6s. The overlap indicates the hybridization of Pb 6s and 6p orbitals in this energy range. This contrasts with the dominance of the Pb-6s character throughout the valence band of $Pb(Tt)_2$. There is a small amount of Pb-6p PDOS at −2 eV, which does not overlap with the PDOS of Pb-6s. Thus, the 6s-6p orbital hybridization is negligible in $Pb(Tt)_2$, preserving the isotropic character of the filled Pb-6s orbital. We also quantified the magnitude of the LP activity of these compounds using the framework of bond-valence analysis of solids with active LPs.[39–42] The LP vector ($\boldsymbol{\Phi}$) defined in these analyses can be used as an indicator of the strength of the LPs on Pb^{2+}. The averaged vector length $|\boldsymbol{\Phi}|$ of each Pb site are $|\boldsymbol{\Phi}| = 1.30(1)\times10^{-5}$ (Az = Im), $9.3(1)\times10^{-6}$ (Tr), and 6.37×10^{-22} (Tt), respectively (Figure S6 in SI). Here we notice that the LP activity of $Pb(Az)_2$ decreases as the n_C increases, and becomes essentially zero in $Pb(Tt)_2$. Thus, it was demonstrated that the n_C is preprogramable by appropriate ligand design and that the degree of the 6s-6p mixing can be controlled by n_C. Pre-

served Pb 6s character resulted in dispersive valence bands in $Pb(Tt)_2$.

4.2 VBM of $Pb(Tt)_2$ Is Shallow Enough to Be p-Doped.

In general, dispersive valence bands are indicative of strong bonding and antibonding interaction of orbitals, the latter causing the shallowing of VBM relative to the vacuum level.[43] The depth of a VBM is an important indicator of p-type doping capability, with p-doping becoming easier as a VBM becomes shallower. Using a DFT method, we estimated the depth of the VBMs of $Pb(Az)_2$ by aligning the energy of these Pb 5d orbitals set at the same energy as α-PbO, whose VBM energy is experimentally known[44] (see SI for the detailed procedure). The analysis suggests that the VBMs of $Pb(Az)_2$ are at −6.1 eV (Az = Tt), −6.0 eV (Tr), and −5.5 eV (Im), respectively (Figure 5). Notably, all $Pb(Az)_2$ compounds have shallow VBMs close to −6 eV, an empirical limit considered to be p-dopable.[37] The shallow VBMs of $Pb(Az)_2$ were experimentally confirmed by photoelectron yield spectroscopy, which indicates that all $Pb(Az)_2$ have the VBM levels shallower than −6 eV (Figure S5). Note that the relative order of the VBM depth of $Pb(Az)_2$ may change due to the possible underestimation of band dispersion by the DFT method.

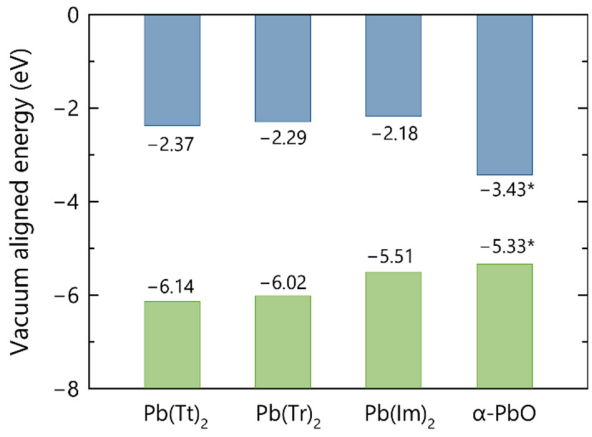

Figure 5. DFT-calculated band edge positions of $Pb(Az)_2$ relative to the vacuum level. Values for α-PbO (with asterisks) are experimental values from the literature.[44]

4.3 Dispersive Valence Band and Shallow VBM of $Pb(Tt)_2$ Are Achieved by Large n_C and Deep-Level MO with Right Symmetry.

In the case of inorganic p-type semiconductors, the HOMO of the anions, the p orbitals, interacts with filled metal orbitals such as s or d. In contrast, it remains to be seen which state of the anions will produce the important interaction in our hybrid compounds due to the complexity of the MOs. The presence of Pb-6s state near the valence band top of $Pb(Tt)_2$ indicates that the filled 6s orbital is destabilized by the antibonding interaction with a certain MO of the anion (Figure 4A). Detailed examination of the highest-energy valence band (HVB) at the Γ point reveals that the MO contributing to this state resembles not the anion's HOMO, but rather the HOMO−3 (Figure 6A, B). The HOMO−3 is a b_2 orbital as the isolated Tt anion belongs to the point group C_{2v}. This orbital alternates in sign on the N atoms of the Tt anion and interacts out-of-phase with the neighboring Pb 6s orbitals, while the HOMO (b_1) of Tt has no net interaction due to symmetry mismatch. For strong σ-type interaction with the Pb 6s orbital, the MOs must be a_1 or b_2 orbitals.

Besides HOMO−3, HOMO−1 (a_1) of the Tt anion appears to have the right symmetry to interact with the Pb 6s orbital (Figure 6B). However, it does not contribute to the HVB due to its suboptimal topology for maximizing nodal planes with the Pb 6s orbital. This results in HOMO−1 contributing to the fifth highest valence state at Γ (HVB−4), partially due to two of the four σ-type interactions are in-phase and bonding (Figure S7 in SI). Thus, the order of the MOs contributing to the valence bands are determined by both orbital symmetry and topology.[45] This energy level inversion of the anion states is unique to hybrid compounds, since in inorganic compounds the filled active orbital of the anions is always *n*p, which has identical symmetry regardless of the elemental species. The energy level inversion is the result of a strong covalent interaction between Pb 6s and HOMO−3 (Figure 6C).

For $Pb(Im)_2$, the character of the wave function near the VBM is dominated by the HOMO (b_1) of the Im anion without contribution from the Pb 6s orbitals (Figure 6D, E). The energy level of the HOMO is so shallow that it forms a localized, flat valence band as a non-bonding state, which becomes the VBM without the help of dispersion (Figure 6F). However, the state at the VBM is not a crystal orbital spread over the entire solid, and it makes little sense to discuss the physical properties of $Pb(Im)_2$ as a semiconductor from its VBM level. This indicates that a shallower energy level of the anion MO is desirable to obtain a shallow VBM, but it results in a localized state when the symmetry of the orbitals does not match. These results suggest that the symmetry of MOs can, in some cases, influence the electronic structure of a hybrid solid more than its energy levels. The impact of MO symmetry has already been highlighted in $Pb(Tt)_2$, but the electronic structure of $Pb(Im)_2$ reaffirms its importance. In the sense that the VBM is formed as non-bonding molecular state, $Pb(Im)_2$ is an ionic crystal.

$Pb(Tr)_2$ shows an intermediate electronic structure between $Pb(Tt)_2$ and $Pb(Im)_2$. The MO contributing to the HVB of $Pb(Tr)_2$ at the Γ point is HOMO−3 (a_1) due to symmetry and topology requirements, similar to the case of $Pb(Tt)_2$ (Figure S8 in SI). However, smaller n_C allows Pb 6p orbital mixing in $Pb(Tr)_2$, which results in an asymmetric coordination geometry and reduced band dispersion.

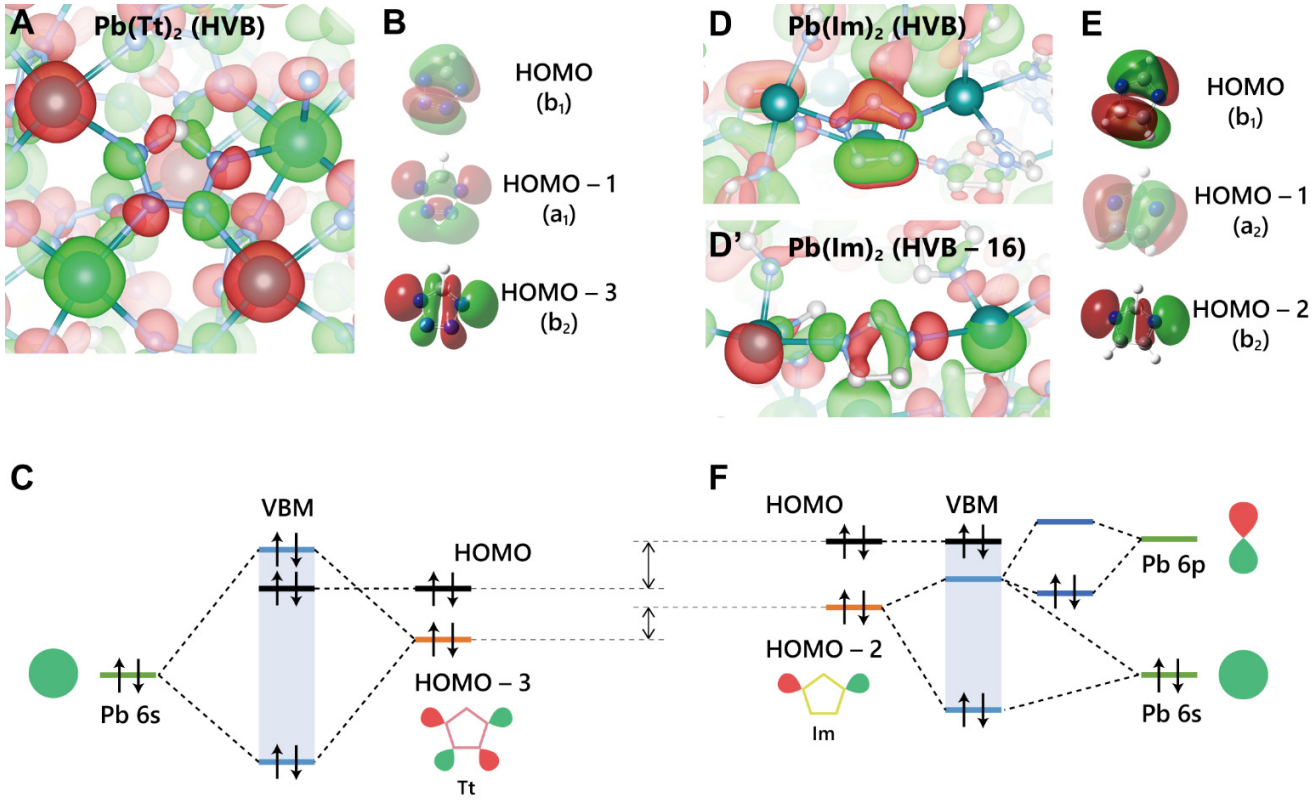

Figure 6. Volumetric visualization for the wave function of (A) highest-energy valence band (HVB) of $Pb(Tt)_2$, (D) HVB of $Pb(Im)_2$, and (D') HVB−16 of $Pb(Im)_2$ (***k*** = Γ). MOs of (B) isolated Tt and (E) isolated Im anions (point group C_{2v}) calculated using Gaussian 16.[46] Schematic interaction diagrams of (C) $Pb(Tt)_2$ and (F) $Pb(Im)_2$. The relative energy difference of MOs are highlighted by arrows. Note that these differences are not scaled to actual energy differences.

4.4 Comparison of Electronic Structures of Hybrid and Inorganic Semiconductors and Usefulness of the Concept of Controlling n_C.

We have started with the simple concept of controlling n_C to obtain an isotropic coordination structure of Pb^{2+} and dispersive valence bands derived from preserved 6s character. The Az anions made this possible by varying the number of N atoms in the ring. However, we explicitly state here that changing the number of N atoms also changes the pristine energy levels of the anion MOs. Since the N atoms are more electronegative than the C atoms, the energy levels of MOs decrease as the number of N atoms in aromatic rings increases.[47,48] This results in a tendency for the MO energy levels to be lower for Im, Tr, and Tt anions, in that order (Figure S9 in SI). This effect is most apparent in the depth of the VBMs of $Pb(Az)_2$ (Figure 5). Although it is in the p-dopable range, the VBM of $Pb(Tt)_2$ estimated by DFT is the deepest of the three $Pb(Az)_2$ due to the deeper MO levels of the Tt anion, despite achieving the largest dispersion. Antibonding interaction between Pb 6s and a higher energy MO could lead to shallower VBMs, even if the dispersion is poor (Figure 6F), which is the case for $Pb(Im)_2$ and $Pb(Tr)_2$.

Thus, it is evident that we cannot decouple the number of the donor site of the anions from the variation of the MO energy levels inherent to the anions. Nonetheless we will show that the concept of controlling n_C remains useful. Note that the dispersive valence band and shallow VBM of $Pb(Tt)_2$ are achieved by fulfilling the following three factors simultaneously:

1. The 6s character of Pb^{2+} is preserved by forcing large n_C (isotropy).
2. There is an MO with an energy level close to Pb 6s (energy matching).
3. The symmetry and topology of the MO are consistent with Pb 6s (shape matching).

Condition 1 gives isotropy, while conditions 2 and 3 give covalency of the coordination bond. In the following discussion, we will highlight the uniqueness of the hybrid system that achieves the coexistence of these two characteristics by comparing it to the electronic structure of inorganic semiconductors.

In binary inorganic compounds containing Pb^{2+}, the covalency of coordination bonds is associated with asymmetric coordination geometry. The DFT study of α-PbO and PbS indicates that the mixing of the Pb 6s and 6p orbitals occurs, if any, through interaction with the p orbital of the anion atoms.[49] Thus, for atomic compounds, the energy level of the anion p states, which interact with metal s orbitals, is a primary factor in determining the degree of Pb-6p mixing or LP formation. For example, LP is formed in α-PbO, while it is not formed in PbS and compounds with higher period chalcogens.[49] This is because the energy level of the 3p orbital of S is already too high to covalently interact with the 6s orbital of Pb to gain sufficient stabiliza-

tion. To compensate for the lack of stabilization energy from orbital hybridization, PbS adopts a more isotropic and dense structure, resulting in a preference for higher coordination number.

The covalency of Pb-6s and O-2p in α-PbO pushes up the 6s state by antibonding interaction, which makes it possible for Pb-6p to mix into this state (Figure S10). In the case of hybrid system, it is remarkable that the covalency of Pb-6s and the HOMO−3 in $Pb(Tt)_2$ does not induce the Pb-6p mixing. We attribute the coexistence of the isotropy and covalency in the coordination bond to the robustness of ligand-based control of n_C. Thus, the large n_C make the system insensitive to the covalency or pristine energy levels of the anion MOs. Although we cannot decouple the number of the donor site of the anions from the variation of the MO energy levels, the control of n_C is robust enough to silence the latter effect.

The abovementioned scheme also explains why the least covalent $Pb(Im)_2$ exhibits the most anisotropic coordination geometry. Lack of covalency results in a more isotropic structure in the inorganic compound, PbS. However, in the 17th valence band of $Pb(Im)_2$, a σ-type antibonding interaction is found between Pb 6s/6p orbitals and the anion's HOMO−2 (Figure 6D', E). The HOMO−2 (b_2) of Im is the highest-energy MO that has the right symmetry for σ-type interaction. The antibonding interaction is not strong enough to push the HOMO−2 up close to the top of the valence band, since its energy level is still shallower compared to the MOs of the Tt anion (Figure S9 in SI). Note that the small n_C of $Pb(Im)_2$ makes it easier to introduce anisotropy in the coordination geometry for Pb 6p mixing. The mixing of the Pb-6p orbital pulls down the energy level (stabilization) and reduces the band dispersion.

Finally, we emphasize the benefit of achieving dispersive valence bands and shallow VBMs using second period elements, because they enable the synthesis of wide gap materials. For inorganic compounds, the VBM energy positions are deepest for oxides and become shallower as the anion period increases as seen in sulfides and selenides. Hybrid materials can take a similar approach, as seen in semiconductors such as $Pb_3(C_6S_6)$.[50] However, the use of higher period elements often results in smaller band gap energy. When high optical transparency or breakdown voltage is required, we need an alternative method to achieve both wide gap and dispersive bands. The second period elements alone cannot achieve this, but we showed that it is possible by being molecules. We have presented one such method in this paper, and the detailed electronic structure analysis discussed here will help to further develop this molecular method.

5. CONCLUSION

While hybrid semiconducting materials with ns^2np^0 metal ions would offer an attractive electronic structure, controlling their valence band dispersion and effective mass of holes are an evolving issue. We started with the simple concept of changing the number of N atoms in azoles to preprogramme the n_C, and indeed succeeded in controlling the n_C and coordination geometry of Pb^{2+} in hybrid crystals. The method thus made it possible to obtain a dispersive valence band (small m_h^*) with a shallow VBM and wide band gap. Furthermore, by examining the wave function of the crystal orbitals of $Pb(Az)_2$ and the MOs of the anions, we were able to clarify the key factors for valence band dispersion and VBM shallowing in these compounds. The analysis of the electronic structure of $Pb(Tt)_2$ reveals an energy-level inversion in which the primary interaction occurs at a much deeper level than the HOMOs of the molecules. Briefly, this phenomenon stems from to the inherent diversity (rich symmetry and topology) of the molecular anions.

We emphasize that the approach of controlling the coordination number by molecular design was robust enough to make the system insensitive to the degree of covalency. This robustness prevents the Pb 6p orbital mixing into the VBM of $Pb(Tt)_2$ while a right-symmetry anion MO having close energy to the Pb-6s orbital, resulting in the compatibility of a large band dispersion, shallow VBM, and wide band gap. Such unconventionality would not be possible with simple atomic orbitals alone and represents a new frontier in materials design in organic-inorganic hybrid solids. There remains the possibility of manipulating the energy, symmetry, and topology of a particular MO by functionalizing the anions with electron withdrawing or donating groups at appropriate positions. Moreover, this molecular approach also offers the potential for engineering conduction band minima, as we observe that the high electronegativity of the N atoms pulls down the unoccupied MOs (N-2p) energy levels lower than the Pb-6p bands in $Pb(Tt)_2$ (Figure 2). Such approaches will be an exquisite extension of this work, and we have established an important foundation for it.

ASSOCIATED CONTENT

Supporting Information. Experimental and computational details, elemental analysis, crystallographic data, PXRD, absorption spectra, photoconductance, and photoelectron yield spectra. This material is available free of charge via the Internet at http://pubs.acs.org. The CIFs for $Pb(Tt)_2$, $Pb(Tr)_2$, and $Pb(Im)_2$ has been deposited in the Cambridge Crystallographic Data Centre with CCDC numbers 2383877, 2383878, and 2383879, respectively.

AUTHOR INFORMATION

Corresponding Author

*E-mail: umeyama.daiki@nims.go.jp

Author Contributions

The manuscript was written through contributions of all authors.

Notes

The authors declare no competing financial interest.

Funding Sources

This work was supported by JSPS KAKENHI Grant Numbers JP24K08460 and JP21H04612.

ACKNOWLEDGMENT

Part of this work was performed at the Surface and Bulk Analysis Unit. The DFT calculations were performed on the Numerical Materials Simulator. These are shared facilities at the National Institute for Materials Science (NIMS). We thank Dr.

Junko Aimi, Dr. Kenji Sakamoto, Dr. Tetsushi Taguchi, Dr. Takeo Ohsawa, and Dr. Hiroshi Mizoguchi (NIMS) for access to equipment.

ABBREVIATIONS

CP, coordination polymer; MOF, metal-organic framework; TM, transition metal; pTM, post-transition metal; LP, lone pair; MO, molecular orbital; CSD, Cambridge Structural Database; DFT, density functional theory; Az, azolate; Tt, tetrazolate; Tr, triazolate; Im, imidazolate; XRD, X-ray diffraction; SCO, spin-orbit coupling; VBM, valence band maximum; PDOS, partial density of states; HVB, highest-energy valence band; n_C, coordination number; m_h^*, effective mass of holes; E_F, Fermi energy; G, conductance; $\boldsymbol{\Phi}$, lone pair vector; a_0, Bohr radius; $\boldsymbol{k}$, wave vector

REFERENCES

(1) Kitai, A. Semiconductor Physics. In *Principles of Solar Cells, LEDs and Diodes: The role of the PN junction*; John Wiley & Sons, Ltd, 2011; pp 1–67.

(2) Aykanat, A.; Meng, Z.; Stolz, R. M.; Morrell, C. T.; Mirica, K. A. Bimetallic Two-Dimensional Metal–Organic Frameworks for the Chemiresistive Detection of Carbon Monoxide. *Angew. Chem. Int. Ed.* **2022**, *61* (6), e202113665. https://doi.org/10.1002/anie.202113665.

(3) Huang, J.; Davenport, A. M.; Heffernan, K.; Debela, T. T.; Marshall, C. R.; McKenzie, J.; Shen, M.; Hou, S.; Mitchell, J. B.; Ojha, K.; Hendon, C. H.; Brozek, C. K. Electrochemical Anion Sensing Using Conductive Metal–Organic Framework Nanocrystals with Confined Pores. *J. Am. Chem. Soc.* **2024**. https://doi.org/10.1021/jacs.4c06669.

(4) Dan-Hardi, M.; Serre, C.; Frot, T.; Rozes, L.; Maurin, G.; Sanchez, C.; Férey, G. A New Photoactive Crystalline Highly Porous Titanium(IV) Dicarboxylate. *J. Am. Chem. Soc.* **2009**, *131* (31), 10857–10859. https://doi.org/10.1021/ja903726m.

(5) Kamakura, Y.; Yasuda, S.; Hosokawa, N.; Nishioka, S.; Hongo, S.; Yokoi, T.; Tanaka, D.; Maeda, K. Selective CO2-to-Formate Conversion Driven by Visible Light over a Precious-Metal-Free Nonporous Coordination Polymer. *ACS Catal.* **2022**, *12* (16), 10172–10178. https://doi.org/10.1021/acscatal.2c02177.

(6) Walte, A. F.; Torres-Cadena, R.; Dayaratne, W. L. N.; Jaffe, A. Mixed-Metal Alloying in Hybrid Bronzes. *J. Am. Chem. Soc.* **2024**, *146* (34), 23699–23703. https://doi.org/10.1021/jacs.4c08960.

(7) Hendon, C. H.; Tiana, D.; Walsh, A. Conductive Metal–Organic Frameworks and Networks: Fact or Fantasy? *Phys. Chem. Chem. Phys.* **2012**, *14* (38), 13120–13132. https://doi.org/10.1039/C2CP41099K.

(8) Givaja, G.; Amo-Ochoa, P.; Gómez-García, C. J.; Zamora, F. Electrical Conductive Coordination Polymers. *Chem. Soc. Rev.* **2011**, *41* (1), 115–147. https://doi.org/10.1039/C1CS15092H.

(9) Sun, L.; Campbell, M. G.; Dincă, M. Electrically Conductive Porous Metal–Organic Frameworks. *Angew. Chem. Int. Ed.* **2016**, *55* (11), 3566–3579. https://doi.org/10.1002/anie.201506219.

(10) Xie, L. S.; Skorupskii, G.; Dincă, M. Electrically Conductive Metal–Organic Frameworks. *Chem. Rev.* **2020**, *120* (16), 8536–8580. https://doi.org/10.1021/acs.chemrev.9b00766.

(11) Singh, N.; Gupta, S.; Sinha, R. K. Preparation, Characterization and Electrical Conductances of Heterometallic Coordination Polymers and Complex Bimetallic Salts Derived from Isomaleonitriledithiolate. *Inorg. Chem. Commun.* **2003**, *6* (4), 416–422. https://doi.org/10.1016/S1387-7003(02)00798-0.

(12) Park, J. G.; Aubrey, M. L.; Oktawiec, J.; Chakarawet, K.; Darago, L. E.; Grandjean, F.; Long, G. J.; Long, J. R. Charge Delocalization and Bulk Electronic Conductivity in the Mixed-Valence Metal–Organic Framework Fe(1,2,3-Triazolate)$_2$(BF$_4$)$_x$. *J. Am. Chem. Soc.* **2018**, *140* (27), 8526–8534. https://doi.org/10.1021/jacs.8b03696.

(13) Cox, P. A. Electronic Energy Levels and Chemical Bonding. In *The Electronic Structure and Chemistry of Solids*; Oxford University Press: Oxford, 1987.

(14) Huang, X.; Fu, S.; Lin, C.; Lu, Y.; Wang, M.; Zhang, P.; Huang, C.; Li, Z.; Liao, Z.; Zou, Y.; Li, J.; Zhou, S.; Helm, M.; St. Petkov, P.; Heine, T.; Bonn, M.; Wang, H. I.; Feng, X.; Dong, R. Semiconducting Conjugated Coordination Polymer with High Charge Mobility Enabled by "4 + 2" Phenyl Ligands. *J. Am. Chem. Soc.* **2023**, *145* (4), 2430–2438. https://doi.org/10.1021/jacs.2c11511.

(15) Kawazoe, H.; Yasukawa, M.; Hyodo, H.; Kurita, M.; Yanagi, H.; Hosono, H. P-Type Electrical Conduction in Transparent Thin Films of CuAlO$_2$. *Nature* **1997**, *389* (6654), 939–942. https://doi.org/10.1038/40087.

(16) Ogo, Y.; Hiramatsu, H.; Nomura, K.; Yanagi, H.; Kamiya, T.; Hirano, M.; Hosono, H. P-Channel Thin-Film Transistor Using p-Type Oxide Semiconductor, SnO. *Appl. Phys. Lett.* **2008**, *93* (3), 032113. https://doi.org/10.1063/1.2964197.

(17) Griffin, S. L.; Champness, N. R. A Periodic Table of Metal-Organic Frameworks. *Coord. Chem. Rev.* **2020**, *414*, 213295. https://doi.org/10.1016/j.ccr.2020.213295.

(18) Orgel, L. E. The Stereochemistry of B Subgroup Metals. Part II. The Inert Pair. *J. Chem. Soc.* **1959**, 3815–3819. https://doi.org/10.1039/JR9590003815.

(19) Walsh, A.; Payne, D. J.; Egdell, R. G.; Watson, G. W. Stereochemistry of Post-Transition Metal Oxides: Revision of the Classical Lone Pair Model. *Chem. Soc. Rev.* **2011**, *40* (9), 4455–4463. https://doi.org/10.1039/C1CS15098G.

(20) Watson, G. W.; Parker, S. C. Origin of the Lone Pair of α-PbO from Density Functional Theory Calculations. *J. Phys. Chem. B* **1999**, *103* (8), 1258–1262. https://doi.org/10.1021/jp9841337.

(21) Watson, G. W. The Origin of the Electron Distribution in SnO. *J. Chem. Phys.* **2001**, *114* (2), 758–763. https://doi.org/10.1063/1.1331102.

(22) Imran, M.; Mix, A.; Neumann, B.; Stammler, H.-G.; Monkowius, U.; Gründlinger, P.; Mitzel, N. W. Hemi- and Holo-Directed Lead(II) Complexes in a Soft Ligand Environment. *Dalton Trans.* **2014**, *44* (3), 924–937. https://doi.org/10.1039/C4DT01406E.

(23) Wu, X.-S.; Tang, Y.-R.; Liu, J.-L.; Wang, L.; Ren, X.-M. Comprehensively Understanding the Steric Hindrance Effect on the Coordination Sphere of Pb^{2+} Ions and Photophysical Nature of Two Luminescent Pb(II)-Coordination Polymers. *Dalton Trans.* **2019**, *48* (36), 13841–13849. https://doi.org/10.1039/C9DT02928A.

(24) Hui, Y.-Y.; Bai, C.; Hu, H.-M.; Lv, B.; Wang, X. The Effects of the Coordination Orientation and Steric Hindrance of Ligands on the Structural Diversity of Pb(II) Coordination Polymers. *Inorganica Chim. Acta* **2020**, *510*, 119751. https://doi.org/10.1016/j.ica.2020.119751.

(25) Zhang, L.; Li, Z.-J.; Lin, Q.-P.; Qin, Y.-Y.; Zhang, J.; Yin, P.-X.; Cheng, J.-K.; Yao, Y.-G. Synthesis, Structure, and Luminescent Properties of Hybrid Inorganic–Organic Framework Materials Formed by Lead Aromatic Carboxylates: Inorganic Connectivity Variation from 0D to 3D. *Inorg. Chem.* **2009**, *48* (14), 6517–6525. https://doi.org/10.1021/ic900425r.

(26) Hu, M.-L.; Morsali, A.; Aboutorabi, L. Lead(II) Carboxylate Supramolecular Compounds: Coordination Modes, Structures and Nano-Structures Aspects. *Coord. Chem. Rev.* **2011**, *255* (23), 2821–2859. https://doi.org/10.1016/j.ccr.2011.05.019.

(27) Savage, M.; Yang, S.; Suyetin, M.; Bichoutskaia, E.; Lewis, W.; Blake, A. J.; Barnett, S. A.; Schröder, M. A Novel Bismuth-Based Metal–Organic Framework for High Volumetric Methane and Carbon Dioxide Adsorption. *Chem. – Eur. J.* **2014**, *20* (26), 8024–8029. https://doi.org/10.1002/chem.201304799.
(28) Kamakura, Y.; Fujisawa, S.; Takahashi, K.; Toshima, H.; Nakatani, Y.; Yoshikawa, H.; Saeki, A.; Ogasawara, K.; Tanaka, D. Redox-Active Tin Metal–Organic Framework with a Thiolate-Based Ligand. *Inorg. Chem.* **2021**, *60* (17), 12691–12695. https://doi.org/10.1021/acs.inorgchem.1c01725.
(29) Shimoni-Livny, L.; Glusker, J. P.; Bock, C. W. Lone Pair Functionality in Divalent Lead Compounds. *Inorg. Chem.* **1998**, *37* (8), 1853–1867. https://doi.org/10.1021/ic970909r.
(30) Davidovich, R. L.; Stavila, V.; Marinin, D. V.; Voit, E. I.; Whitmire, K. H. Stereochemistry of Lead(II) Complexes with Oxygen Donor Ligands. *Coord. Chem. Rev.* **2009**, *253* (9), 1316–1352. https://doi.org/10.1016/j.ccr.2008.09.003.
(31) Satchell, J. F.; Smith, B. J. Calculation of Aqueous Dissociation Constants of 1,2,4-Triazole and Tetrazole: A Comparison of Solvation Models. *Phys. Chem. Chem. Phys.* **2002**, *4* (18), 4314–4318. https://doi.org/10.1039/B203118C.
(32) Zhang, J.-P.; Zhang, Y.-B.; Lin, J.-B.; Chen, X.-M. Metal Azolate Frameworks: From Crystal Engineering to Functional Materials. *Chem. Rev.* **2012**, *112* (2), 1001–1033. https://doi.org/10.1021/cr200139g.
(33) Ouellette, W.; Hudson, B. S.; Zubieta, J. Hydrothermal and Structural Chemistry of the Zinc(II)- and Cadmium(II)-1,2,4-Triazolate Systems. *Inorg. Chem.* **2007**, *46* (12), 4887–4904. https://doi.org/10.1021/ic062269a.
(34) Perdew, J. P.; Burke, K.; Ernzerhof, M. Generalized Gradient Approximation Made Simple. *Phys. Rev. Lett.* **1996**, *77* (18), 3865–3868. https://doi.org/10.1103/PhysRevLett.77.3865.
(35) Kresse, G.; Furthmüller, J. Efficient Iterative Schemes for Ab Initio Total-Energy Calculations Using a Plane-Wave Basis Set. *Phys. Rev. B - Condens. Matter Mater. Phys.* **1996**, *54* (16), 11169–11186. https://doi.org/10.1103/PhysRevB.54.11169.
(36) Kresse, G.; Furthmüller, J. Efficiency of Ab-Initio Total Energy Calculations for Metals and Semiconductors Using a Plane-Wave Basis Set. *Comput. Mater. Sci.* **1996**, *6* (1), 15–50. https://doi.org/10.1016/0927-0256(96)00008-0.
(37) Hosono, H. Exploring Electro-Active Functionality of Transparent Oxide Materials. *Jpn. J. Appl. Phys.* **2013**, *52* (9R), 090001. https://doi.org/10.7567/JJAP.52.090001.
(38) Kitai, A. *Principles of Solar Cells, LEDs and Diodes: The Role of the PN Junction*; John Wiley & Sons, Ltd, 2011; p 43.
(39) Brown, I. D. Chemical and Steric Constraints in Inorganic Solids. *Acta Crystallogr. B* **1992**, *48* (5), 553–572. https://doi.org/10.1107/S0108768192002453.
(40) O'Keeffe, M.; Brese, N. E. Bond-Valence Parameters for Anion-Anion Bonds in Solids. *Acta Crystallogr. B* **1992**, *48* (2), 152–154. https://doi.org/10.1107/S0108768191013083.
(41) Wang, X.; Liebau, F. Influence of Lone-Pair Electrons of Cations on Bond-Valence Parameters. *Z. Für Krist. - Cryst. Mater.* **1996**, *211* (7), 437–439. https://doi.org/10.1524/zkri.1996.211.7.437.
(42) Wang, X.; Liebau, F. Studies on Bond and Atomic Valences. I. Correlation between Bond Valence and Bond Angles in Sb^{III} Chalcogen Compounds: The Influence of Lone-Electron Pairs. *Acta Crystallogr. B* **1996**, *52* (1), 7–15. https://doi.org/10.1107/S0108768195004472.
(43) Ogawa, K.; Abe, R.; Walsh, A. Band Gap Narrowing by Suppressed Lone-Pair Activity of Bi^{3+}. *J. Am. Chem. Soc.* **2024**. https://doi.org/10.1021/jacs.4c00150.
(44) Majima, E.; Kozuka, Y.; Uchida, M.; Nakamura, M.; Kawasaki, M. Band Alignment and Photovoltaic Effect of Epitaxial α-PbO Thin Films. *Appl. Phys. Express* **2015**, *8* (7), 074001. https://doi.org/10.7567/APEX.8.074001.
(45) Hoffmann, R. How Chemistry and Physics Meet in the Solid State. *Angew. Chem. Int. Ed. Engl.* **1987**, *26* (9), 846–878. https://doi.org/10.1002/anie.198708461.
(46) Frisch, M. J.; Trucks, G. W.; Schlegel, H. B.; Scuseria, G. E.; Robb, M. A.; Cheeseman, J. R.; Scalmani, G.; Barone, V.; Petersson, G. A.; Nakatsuji, H.; *et al*. Gaussian 16, Revision C.01, Gaussian, Inc., Wallingford CT, 2019.
(47) Kaim, W. The Versatile Chemistry of 1,4-Diazines: Organic, Inorganic and Biochemical Aspects. *Angew. Chem. Int. Ed. Engl.* **1983**, *22* (3), 171–190. https://doi.org/10.1002/anie.198301713.
(48) Chen, D.; Su, S.-J.; Cao, Y. Nitrogen Heterocycle-Containing Materials for Highly Efficient Phosphorescent OLEDs with Low Operating Voltage. *J. Mater. Chem. C* **2014**, *2* (45), 9565–9578. https://doi.org/10.1039/C4TC01941E.
(49) Walsh, A.; Watson, G. W. The Origin of the Stereochemically Active Pb(II) Lone Pair: DFT Calculations on PbO and PbS. *J. Solid State Chem.* **2005**, *178* (5), 1422–1428. https://doi.org/10.1016/j.jssc.2005.01.030.
(50) Turner, D. L.; Vaid, T. P.; Stephens, P. W.; Stone, K. H.; DiPasquale, A. G.; Rheingold, A. L. Semiconducting Lead–Sulfur–Organic Network Solids. *J. Am. Chem. Soc.* **2008**, *130* (1), 14–15. https://doi.org/10.1021/ja0770983.

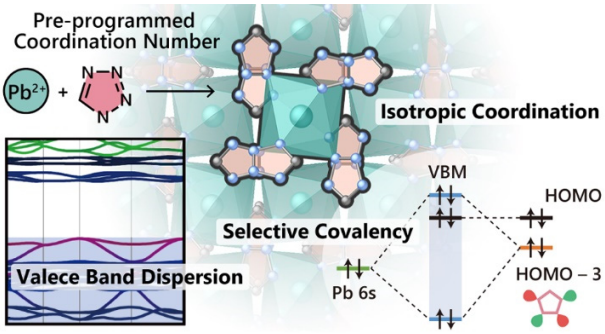
Pre-programmed
Coordination Number
Pb2+
Isotropic Coordination
Selective Covalency
Valece Band Dispersion
VBM
HOMO
HOMO – 3
Pb 6s